Quantified mass loss of the Laohugou ice core and its precipitation signal during 1961–2005 at high elevation in the northeastern Tibetan Plateau

Wentao Du[1,2], Shichang Kang[1,2], Jizu Chen[1], Weijun Sun[3], Xiang Qin[1], Zhenming Ji[4,5], Wenxuan Sun[1,4] and Yanan Qiu[1,6]

[1]Qilian Shan Station of Glaciology and Eco-environment, State Key Laboratory of Cryospheric Science, Northwest Institute of Eco-Environment and Resources, Chinese Academy of Sciences (CAS), Lanzhou, China; [2]University of Chinese Academy of Sciences, Beijing, China; [3]College of Geography and Environment, Shandong Normal University, Jinan, China; [4]Guangdong Province Key Laboratory for Climate Change and Natural Disaster Studies, School of Atmospheric Sciences, Sun Yat-sen University, Guangzhou, China; [5]Southern Marine Science and Engineering Guangdong Laboratory (Zhuhai), Zhuhai, China and [6]School of Aerospace Science and Technology, Xidian University, Xi'an, Shaanxi, China

Abstract

Ice records provide a qualitative rather than a quantitative indication of the trend of climate change. Using the bulk aerodynamic method and degree day model, this study quantified ice mass loss attributable to sublimation/evaporation (S/E) and meltwater on the basis of integrated observations (1960–2006) of glacier-related and atmospheric variables in the northeastern Tibetan Plateau. During 1961–2005, the average annual mass loss in the ice core was 95.33 ± 20.56 mm w.e. (minimum: 78.97 mm w.e. in 1967, maximum: 146.67 mm w.e. in 2001), while the average ratio of the revised annual ice accumulation was 21.2 ± 7.7% (minimum: 11.0% in 1992, maximum 44.8% in 2000). A quantitative formula expressing the relationship between S/E and air temperature at the monthly scale was established, which could be extended to estimation of S/E changes of other glaciers in other regions. The elevation effect on alpine precipitation determined using revised ice accumulation and instrumental data was found remarkable. This work established a method for quantitative assessment of the temporal variation in ice core mass loss, and advanced the reconstruction of long-term precipitation at high elevations. Importantly, the formula established for reconstruction of S/E from temperature time series data could be used in other regions.

1. Introduction

Annual ice accumulation reflects the trend of precipitation rather than the actual amount because of ice mass loss caused by various degrees of melting, sublimation/evaporation (S/E) and snowdrifting (Stichler and others, 2001; Kang and others, 2015). Ice loss in the Arctic, Antarctic and middle/low latitudes has been studied comprehensively using energy mass balance models driven by reanalysis data (van den Broeke and others, 2009; Lenaerts and others, 2012; Mölg and others, 2012; Reijmer and others, 2012; van Pelt and others, 2012; Noël and others, 2016). Few studies have conducted similar assessments in relation to the Tibetan Plateau (TP) owing to scarce observations at high elevation and the generally poor performance of reanalysis data for this region (You and others, 2014, 2015, 2019); however, ice core research has been conducted to reconstruct climatic and environmental changes at atmospheric levels equivalent to the height of the TP (Hou and others, 2002; Kang and others, 2015). In comparison with other proxies, sequences of precipitation events are usually well recorded in ice cores because the water is retained directly. However, the recorded precipitation with its embedded isotopic and chemical information can be modified by various post-depositional processes such as wind scour (Fisher and Koerner, 1994), meltwater percolation (Taylor and others, 2001) and refreezing (Zhou and others, 2008), erosive and depositional sublimation (Stichler and others, 2001) and vapor diffusion (Johnsen and others, 2000). Thus, the influence of postdepositional processes should be considered when interpreting precipitation sequences recorded in ice cores.

Recent studies found that glacial shrinkage in western China is more pervasive than previously realized, especially on the TP (Guo and others, 2015; Yao and others, 2012), where even deficits in the accumulation area are observed in certain regions, for example, Geladiandong, Namunani and Tanggula in central and southern parts of the TP (Kang and others, 2015; Zhang and others, 2015). Such findings raise new challenges in relation to ice core studies, and highlight the urgent need both to assess mass loss in ice cores and to identify its governing processes.

Use of ice cores to reconstruct past precipitation variation has been adopted widely in studies in western China (e.g. on the TP, and in the Tien Shan and Altai mountains) because it can enhance understanding of the long-term spatial patterns and evolution of alpine precipitation

(Yao and others, 1996; Hou and others, 2002; Kang, 2011). Additionally, most meteorological observations in northwestern China are taken at locations on low-elevation plains or in river valleys, and provide only short-term precipitation data with uneven distribution (Kang and others, 2010; You and others, 2010). Moreover, horizontal and trace precipitation at high elevations cannot be collected efficiently using the observational instruments currently available (Sun and others, 2018).

Therefore, consideration of integrated observations obtained at glacial drilling sites would provide opportunities for precise quantification of the amount of ice mass loss, and promote understanding regarding precipitation in alpine regions (or at high elevations). It would also support sustainable use of regional water resources and the development of land-use patterns in arid northwestern China (Immerzeel and Bierkens, 2012; Cauvy and others, 2016; Qin and others, 2017).

To quantitatively investigate ice loss and precipitation variations with consideration of depositional processes, this study assessed the climatic indictors (1960–2006) of the Laohugou (LHG) ice core (Cui and others, 2010) in terms of the evolution from snow to ice, in situ mass balance, and climatological change, and analyzed the relationships with local meteorological and topographical conditions. In the LHG Glacier No. 12 region, one such integrated observation network established in 2008 is operated by the Qilian Shan Station of Glaciology and Eco-environment (Chinese Academy of Sciences). The network obtains routine observations of the glacier, and the local atmosphere, hydrology and ecology. In this study, the primary processes of ice mass loss that comprise S/E and meltwater loss were quantified using the bulk aerodynamic method (BAM) and the degree day model (DDM) on the basis of in situ S/E, mass balance, automatic weather station (AWS) and interpolated air temperature time series data. The influence of wind speed was considered in the BAM, but mass loss attributed to snowdrifting was neglected owing to its minimal impact (i.e. approximately only several millimeters water equivalent) (Gascoin and others, 2013; Zhou and others, 2013; Mott and others, 2018; Pramanik and others, 2019). Furthermore, the effect of snow avalanches was also neglected because the study site is in a large reasonably flat area (slope: ∼3°). Owing to the urgency of the need to assess mass loss in ice cores under the background of unprecedented glacial shrinkage, we used very scarce integrated observations to quantify the mass loss of an ice core from the northeastern TP to gain accurate understanding of the variations in alpine precipitation at high elevations.

2. Material and methods

2.1. Study region

This study was conducted on LHG Glacier No. 12 (39°26.4′N, 96°32.5′E; RGI 60-13.33006, Fig. 1), which was the first designated monitoring glacier in China owing to it being an extreme-continental type glacier and the largest valley glacier in the Qilian Mountains. The Qilian Shan Station originally operated from 1958 until 1962, but was then recommissioned in 2008. In 2006, a shallow ice core was retrieved at the firn basin (elevation: 5040 m a.s.l.), where the annual air temperature on the glacier surface is −11.8°C, annual precipitation is ∼424 mm w.e., melting is minimal (Sun and others, 2012; Chen and others, 2018), and ice flow is slow owing to the relatively flat terrain (Du and others, 2016a).

2.2. Data

2.2.1. Automatic weather station meteorological dataset
One AWS-C (red flag in Fig. 1) was deployed at the drilling site (39°25′39.5″N, 96°33′21.8″E; 5040 m a.s.l.) on LHG Glacier No. 12 in 2009. Air temperature, relative humidity, wind speed and wind direction were measured at two heights (1.5 and 3 m). Air pressure, incoming shortwave radiation, reflected shortwave radiation, incoming longwave radiation and outgoing longwave radiation were measured at one height (1.5 m). Measurements were taken synchronously every 10 s, and 30-min means of the measurements were recorded. Two similar AWSs operated in the ablation region (yellow flag in Fig. 1, 4550 m a.s.l.) and base camp (green flag in Fig. 1, 4260 m a.s.l.) during 2009–2015. Maintenance of the AWSs was conducted twice monthly during May–October each year. Because meteorological observations might contain errors resulting from nonconsecutive measurements, outliers and missing data, several methods were adopted prior to data analysis to eliminate erroneous data and to fill missing values (Sun and others, 2017). Erroneous data were manually checked, validated and corrected or removed. Missing precipitation data over a period of one or two days were filled using the average precipitation values of neighboring days; if more than two consecutive days had missing data, the missing values were replaced with the long-term averages for the same days.

2.2.2. Mass balance
Determination of the annual mass balance using the direct glaciological method relies on repeated measurements taken at stakes and snow pits on the glacier surface. Glacier ablation can be obtained by subtraction between the observed mass balance and mass accumulation (solid precipitation). Near to the drilling site, three stakes were placed to measure the relative change of snow surface height, and snow pits were dug to measure the depth and density of different snow layers to obtain water equivalent values. Those observations were conducted at intervals to calculate the mass balance by combining changes of snow surface height and water equivalent values from the snow pits. In this work, the observations were performed at the drilling site at one-month intervals during May–September in 2011 and 2012.

2.2.3. Reconstruction of monthly air temperature during 1958–2008
We collected observational temperature data in the LHG glacier region (1959–1961, 2008–2009) and from six meteorological stations (Duanhuang, Yumenzhen, Jiuquan, Tuole, Lenghu and Dachaidan) to reconstruct temperature change at the drilling site. The observations from 1959–1961 were used for calibration, while the in situ temperature data acquired during 2008–2009 were used for validation. First, methods such as ordinary Kriging, inverse distance weighting, spline functions, multiple regression analysis and regional climate model simulations adjusted for elevation were trialed to select the optimal approach, which was ultimately determined as ordinary Kriging. Meanwhile, both the in situ lapse rate at different elevations and the thermocline coefficient between the land and the glacier were also considered. Finally, the temperature change at the drilling site was reconstructed (Du and others, 2011).

2.2.4. LHG ice core
In June 2006, a 20.12 m ice core was retrieved from the firn basin of LHG Glacier No. 12 (39°25′39.5″N, 96°33′21.8″E; 5040 m a.s.l.). It was cut into consecutive 3–5 cm samples at a temperature of −5°C. The oxalate, fluoride and other main ions were analyzed. Oxygen isotope analysis and β activation grade analysis were also performed. Using a multiparameter method based on the seasonal variation characteristics of $\delta^{18}O$, the main ions, the β activity in 1963, and the visible dirty layers deposited during winter and spring seasons, the ice core was dated to the period of 1960–2006, with average resolution of 11–12 samples per year (Du and others, 2016a).
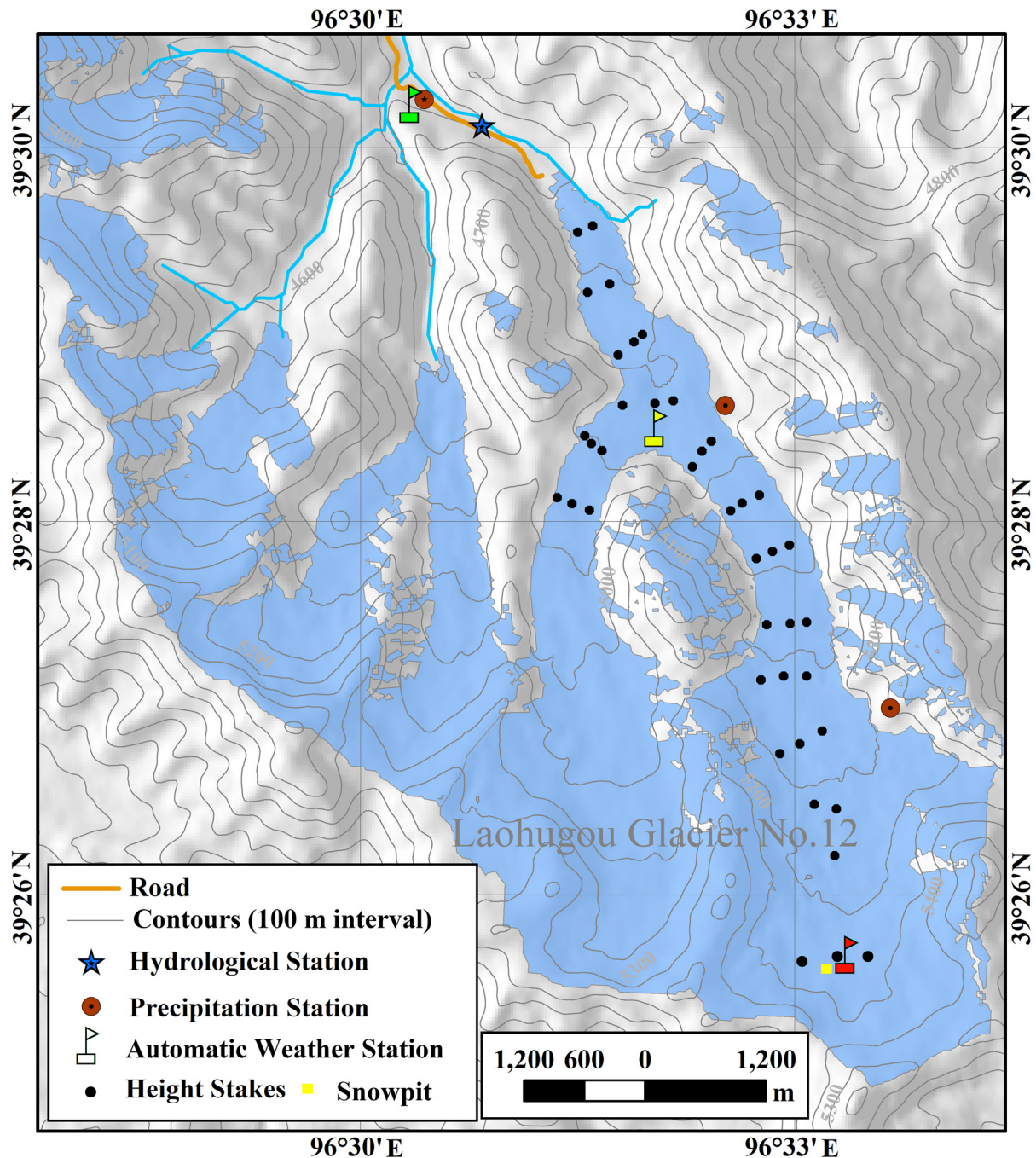
Figure 1. In situ observation network on Laohugou Glacier No. 12.

2.3. Methods

Ice core mass loss is generally attributable to melting, S/E, snow-drifting, and avalanches. In this work, melting and S/E were considered the primary sources of ice mass loss, while the effects of snowdrifting and avalanches were ignored; the reason for this is discussed in section 4.1. Both the DDM and the BAM were used to determine melting and S/E. It should be noted that ice core mass loss was attributed solely to S/E until 1996 because slight melting was fully preserved in the snow pit, as analyzed in section 3.1. After 1996, ice core mass loss consisted of both S/E and melting, as analyzed in section 3.2.2. Because the only meteorological variable that could be obtained is temperature, we constructed a quantitative relationship between temperature and mass loss (S/E & meltwater loss). First, we established a temperature-based S/E reconstruction to obtain S/E during the entire period (see section 3.2.1). Second, the drastic melting

period with meltwater loss was determined using the Mann–Kendall test for positive degree days (PDD) and using the DDM to calculate ablation, from which we subtracted S/E to quantify the meltwater. Using the meltwater freezing ratio determined through a designed contrast test, we obtained the meltwater loss (see section 3.2.2). Further details regarding the methods are described in the following.

2.3.1. Bulk aerodynamic method

Generally, S/E is calculated from the latent heat flux at the glacial surface, which can be determined more accurately based on datasets of on-glacier meteorological measurements than based on off-glacier measurements (Gabbi and others, 2014). The BAM has been used successfully to calculate the latent heat flux on LHG Glacier No. 12 (Sun and others, 2012, 2014, 2017; Chen, 2014). In this study, the BAM was used to calculate the latent heat fluxes

(following Eqn (1)), and the inputs included wind speed and air and glacier surface humidity. The most important parameters in the BAM are the roughness lengths for momentum (Z_{om}), and humidity (Z_{oq}), following Sun and others (2012, 2014).

The analytical expression used for the latent flux was as follows (e.g. Oke, 1987):

$$H = \rho \frac{L_s k^2 u(q - q_s)}{\ln(z/z_{om})\ln(z/z_{oq})}(\Phi_m \Phi_v)^{-1}, \tag{1}$$

where ρ is air density at 5040 m a.s.l., k is the von Karman constant ($k = 0.4$), u and q are wind speed (m s^{-1}), and specific humidity (dimensionless), respectively, at height z, q_s is the surface specific humidity (assumed saturated at the surface), L_s is the latent heat of sublimation of snow or ice (2.834 MJ Kg^{-1}), and Z_{om} and Z_{oq} are the surface roughness lengths (m) for momentum, and humidity, respectively. The nondimensional stability functions for momentum (Φ_m, i.e. 0.9 mm), and moisture (Φ_v) are expressed as a function of the bulk Richardson number including the stability correction (Andreas, 1987; Sun and others, 2012). Roughness is a temporal parameter with a differential spatiotemporal pattern, resulting in uncertainty of the latent heat and sensible heat fluxes. Additionally, the change in the height of the AWS attributable to the ablation also causes error.

2.3.2. Degree day model

The DDM has been applied successfully to estimation of ablation in relation to many glaciers and ice sheets globally (e.g. Braithwaite and Zhang, 2000). The ablation of snow/ice (M) is calculated on the basis of the strength of ablation (DDF) and the sum of the daily mean temperatures above the ablation point (PDD) during a certain period:

$$M = DDF \times PDD, \tag{2}$$

$$PDD = \sum_{t=1}^{n} H_t T_t, \tag{3}$$

where T_t is the daily mean air temperature (°C), and H_t is a logical variable ($H_t = 1$ for $T_t \geq 0$°C and $H_t = 0$ for $T_t < 0$°C).

In this work, some important parameters including the ablation time, DDF, PDD and meltwater refreezing ratio (MRR) were determined following data analysis, as discussed in section 3.2.2.

2.3.3. Mann–Kendall test

In this study, the Mann–Kendall test was used to detect abrupt changes in the long-term data series. However, if the intersection was outside the confidence interval, we employed another method (i.e. the moving t test technique) to analyze the stationarity data. In this approach, UF is the forward sequence that follows the normal distribution, indicating the change trend, while UB can be denoted by reversing the data series based on the same equation. The approximate time of occurrence of the change point can be located according to the intersection between UF and UB within the confidence interval. In this study, testing of the trends was performed with a significance level of $\alpha = 0.05$. In the resulting figure, the y-axis represents the UF and UB results obtained using the Mann–Kendall test (Hamed and Rao, 1998).

3. Results

3.1. Reliability and validity of the LHG ice core

The LHG ice core was extracted from a central position in a large firn basin without steep surrounding mountains on LHG Glacier

No. 12, where the surface was reasonably flat (slope: ∼3°). This site is highly suitable for storing snow and ice because of the minimal ice flow on the decadal timescale and the virtual impossibility of snow avalanches. Furthermore, the annual temperature is approximately −12°C, and there are only approximately 20 days per year (mostly during July and August) when the daily temperature is >0°C. The cold climate allows meltwater to be well stored in the snow layer of the past year, although percolation of meltwater into lower snow layers could occur (Cui and others, 2010, 2014). On LHG Glacier No. 12, glacial winds prevail throughout the year and mountain–valley winds dominate in spring and summer (Du and others, 2012). Although snowdrifting can redistribute some of the surface snow, its contribution to mass change can be considered negligible because only minor differences (i.e. several millimeters water equivalent) have been reported for adjacent regions (Zhou and others, 2013). The depth of the snow pits dug at the drilling site in the summers of 2006, 2008, 2009 and 2010 were in the range of ∼80–200 cm. Snow chemistry analysis revealed evident seasonal variation in both the stable oxygen isotopes and the dust layers of the snow pits (LIGG, 1988; Cui and others, 2014; Yu and others, 2014; Zhang and others, 2017), indicating that annual information could be extracted.

The contribution of S/E to ice core mass change was substantial. The amount of annual melting at the drilling site, calculated using the mass balance and the energy balance model, was ∼110 mm w.e., that is, greater than the measured value attributable to refreezing and far less than the annual accumulation. In terms of homologous consistency between the ice core records and the in situ measurements, it can be concluded that postdepositional effects on the LHG ice core would be sufficiently small to be ignored (Du and others, 2016a, 2016b).

Considering the above discussion, it is recognized that the LHG ice core should be a reasonable indicator of historic climatological and environmental trends. To retrieve actual precipitation, this study considered two principal processes of ice core mass loss: meltwater loss during short melt times and S/E throughout an entire year.

3.2. Quantification of mass loss of the LHG ice core

3.2.1. Mass loss caused by sublimation/evaporation (S/E)

The principal cause of mass loss at the drilling site might be S/E, especially during the cold seasons (Sun and others, 2012). To reconstruct S/E since 1960, it was necessary to establish a relationship between S/E and air temperature because only air temperature data were available for the entire study period.

Latent heat flux at both the accumulation zone during 2011–2012 and the ablation zone during 2009–2015 was calculated using the BAM; full details of the method are described in Sun and others (2012, 2014, 2017). The method included an initial stability correction. Then, connections between monthly mean S/E and monthly mean temperature, wind speed and water vapor pressure were investigated comprehensively (Fig. 2). Although wind speed directly influences latent heat flux, no significant relationship between S/E and wind speed was found (Fig. 2b) owing to the low variability in wind speed (range: 2–4 m s^{-1}). Monthly variation of S/E was similar to that of both water vapor pressure (Fig. 2c) and temperature (Fig. 2a) because water vapor is strongly correlated with temperature in different seasons (Chen and others, 2018). At monthly intervals, S/E was found correlated positively in the cold seasons (January–April and October–December) with air temperature below −4.8°C, whereas S/E was found correlated negatively in the warm seasons (May–September) with air temperature of above −4.8°C (Fig. 2a). There are several reasons for such a relationship between S/E and air temperature. Water vapor pressure on the glacier surface is
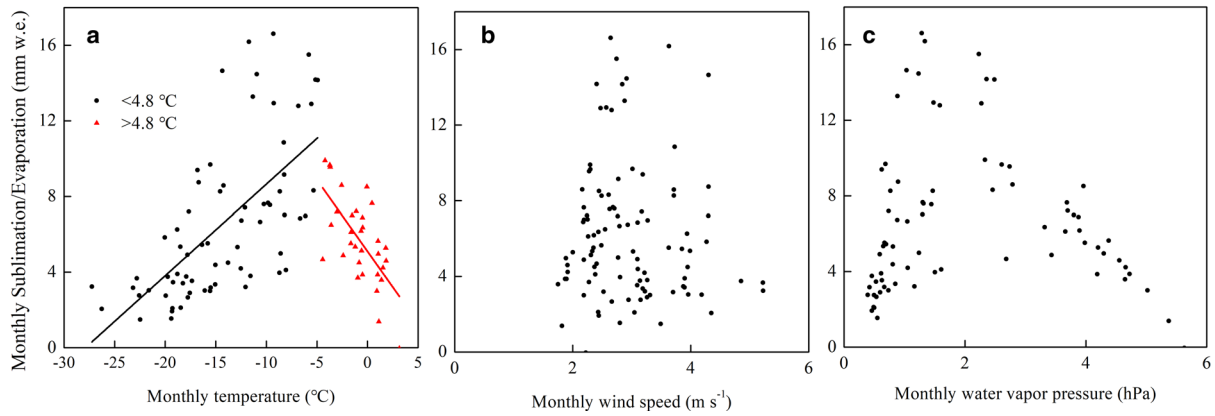
Figure 2. Relationships between monthly sublimation/evaporation (S/E) and monthly average (a) temperature, (b) wind speed and (c) water vapor pressure. Black straight line denotes linear regression between S/E and air temperature when the temperature is below (above) −4.8°C.

always saturated, which is determined by the glacier surface temperature. As shown in (Fig. 2), during months with air temperature of below −4.8°C, the rate of increase of water vapor pressure in the air is slower than that of water vapor pressure on the glacier surface with increasing air temperature. Consequently, the water vapor pressure difference becomes larger, enhancing latent heat and S/E. Thus, S/E will increase following temperature rise in the cold seasons. During months with air temperature of above −4.8°C, with increasing air temperature, the surface ice temperature gradually reaches melting point, resulting in the water vapor pressure on the glacier surface reaching a saturated state corresponding to the melting point temperature, and it finally stops rising. Meanwhile, water vapor pressure in the air increases rapidly with rising temperature, such that the difference in water vapor between the glacier surface and the air decreases, resulting in reduced latent heat (Fig. 2).

Given the distinct connection between S/E and air temperature, monthly S/E since 1960 was reconstructed using only the temperature data in the time series. A series of threshold values from 4–6°C was considered at intervals of 0.2°C, and two linear regressions were performed between S/E and temperature at each interval: one for the negative threshold in the cold seasons and one for the positive threshold in the warm seasons. The best match with the observations was identified at −4.8°C (Fig. 2a), with $r = 0.66$ ($n = 102$, $p < 0.05$) and root mean square error of ± 2.7 mm w.e.

For both the warm–wet and the cold–dry seasons, S/E was reconstructed on the basis of the following regression equations:

$$S/E = 0.484 \times T_m + 13.49 (T_m < -4.8°C), \tag{4}$$

$$S/E = -0.756 \times T_m + 5.10 (T_m > -4.8°C), \tag{5}$$

where T_m is monthly air temperature. As shown in Figure 3a, there was no obvious trend of S/E in the warm–wet seasons prior to 1990, but there was a trend of slight increase after 1990. In the warm–wet seasons, S/E varied from 34.55 mm w.e. (in 1976) to 44.84 mm w.e. (in 1979); the median and mean values were 35.04 and 36.84 ± 1.54 mm w.e., respectively. In the cold–dry seasons (Fig. 3b), S/E increased after 1979 (slope = 0.16 mm w.e. a^{-1}, $p < 0.05$) from 40.21 mm w.e. (in 1979) to 57.1 mm w.e. (in 1998); the median and mean values were 47.89 and 49.87 ± 3.2 mm w.e., respectively. In summary, the highest, lowest, median, and mean values of annual S/E were 95.08 mm w.e. (in 1998), 78.97 mm w.e. (in 1967), 82.93 and 86.71 ± 3.52 mm w.e., respectively (Fig. 3c). Although S/E diminished with increasing temperature in the warm seasons, it appeared to increase with increasing temperature in the longer cold seasons, especially after 1991 (1961–1990: slope = 0.1 mm a^{-1}, failed to pass the confidence test; 1991–2005: slope = 0.31 mm w.e. a^{-1}, $p < 0.05$). Since the 1990s, the increase in S/E during the cold seasons has been stronger than the decrease during the warm seasons (1998–2005: slope = −0.035 mm w.e. a^{-1}, failed to pass the confidence test), resulting in overall annual increase. On the basis of the Mann–Kendall test, we can conclude that this trend of increase from the 1970s had an abrupt change point at 1993. Thus, the average annual S/E was 85.2 mm w.e. before 1992, after which it increased to 90.42 mm w.e. Although S/E was increasing prior to 1992 (slope = 0.106 mm a^{-1}, $p < 0.05$), its rate of increase accelerated markedly after 1992 (slope = 0.438 mm w.e. a^{-1}, $p < 0.05$).

The increase in annual S/E at the drilling site, which is very different to the decline observed elsewhere in the Northern
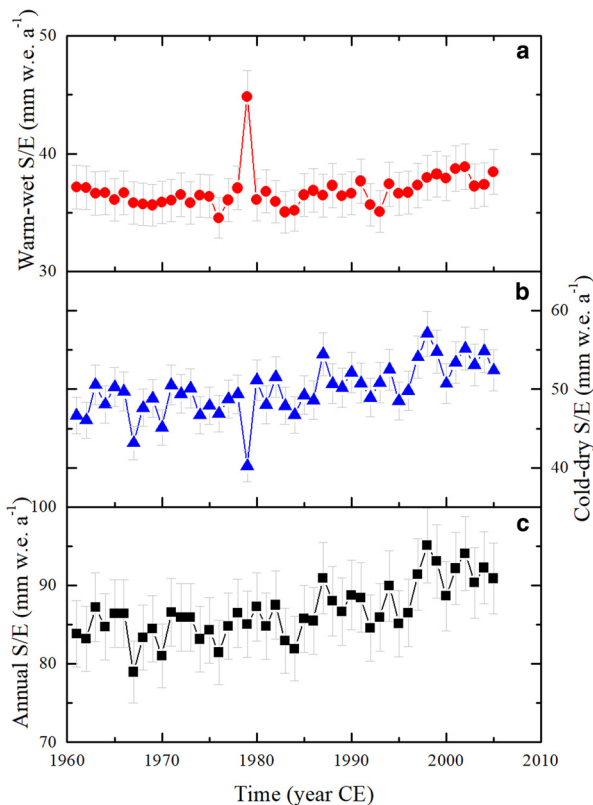

Figure 3. Reconstructed sublimation/evaporation (S/E) since 1960. (a) warm–wet seasons, (b) cold–dry seasons and (c) annually (error bars in gray).

Hemisphere before 1993, can be explained as follows. The foremost reason is the substantial elevation difference. Typically, the higher the elevation, the more intense the solar radiation, the greater the wind speed, and the more dramatic the warming and the supply of water vapor in glacier/snow regions. Such conditions are conducive to higher S/E, especially in regions with elevation of >3000 m a.s.l., as confirmed in a previous study of a semiarid region (Schulz and Jong, 2004). Furthermore, most observations of S/E in the Northern Hemisphere are acquired on plains, and the decreasing trend is weakened or even reversed with increasing elevation. For example, in Xinjiang Province in western China, the decrease in pan evaporation has been more drastic on the plains in comparison with that in alpine regions (Su and others, 2003). The elevation at the drilling site of this study is >5000 m a.s.l., that is, much higher than that of the study site of Su and others (2003). Thus, it is very likely that the trend of S/E at the drilling site is flat or even increasing. The second reason is related to land surface type, for example, snow. The particular characteristics of the snow/ice surface and climate create a relationship of increasing S/E with temperature increase when the monthly air temperature is below −4.8°C. At the high elevation of the drilling site, monthly air temperature has generally always been below −4.8°C during autumn–spring. However, during the past 50 years, air temperature has increased, especially the winter temperature, which has led to increased S/E in those months in which air temperature is below −4.8°C.
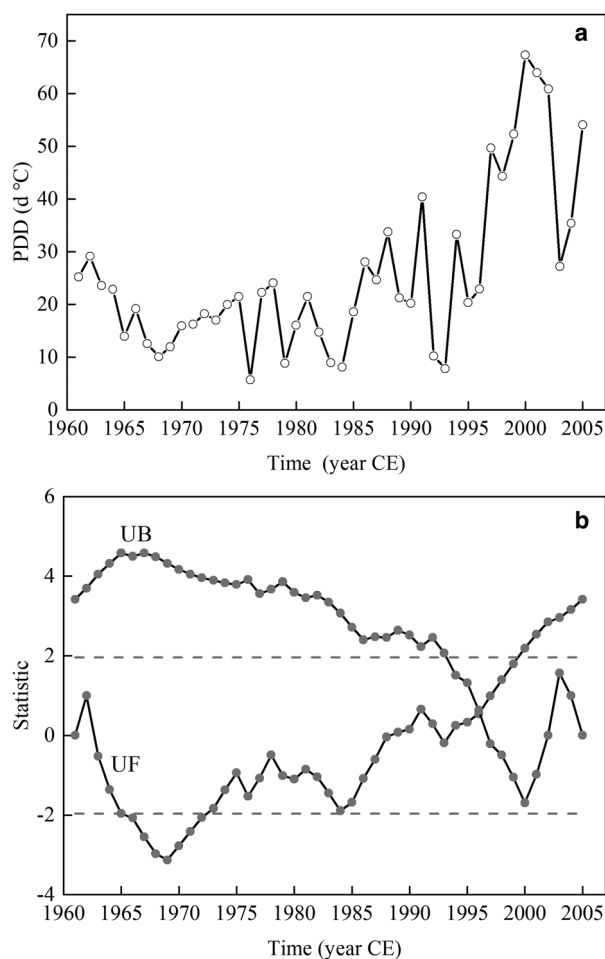
Although S/E in some warm months has diminished with warming, the months with air temperature below −4.8°C account for a larger proportion of the year; thus, the increase in winter air temperature has been more dramatic, leading to overall increase in S/E with global warming.

3.2.2. Mass loss caused by melting

Ice core mass loss attributable to meltwater was obtained by subtracting S/E and the meltwater refreezing from ablation, which can be calculated using the DDM. Total melting was considered to comprise meltwater loss and refreezing. Here, certain crucial points should be considered, for example, the melting condition (i.e. PDD), melting strength (i.e. DDF) and the MRR.

Ablation period: The PDD was calculated using reconstructed monthly temperature time series data for 1957–2008 (Fig. 4a) (Du and others, 2011). The monthly temperature in each year was assumed normally distributed. The Mann–Kendall test identified significant increase in PDD in 1997 (Fig. 4b), indicating temperature fluctuation in a similar range during 1960–1996. Following a previous study focusing on modern evolution processes from snow to ice on LHG Glacier No. 12 (Huang and Xie, 1988), it can be concluded that climatic and environmental information for approximately two years could be well preserved in the snow layers at the drilling site. The Mann–Kendall test also showed that an abrupt change point in cumulative positive temperature occurred in 1996, indicating that significant warming since 1997 has intensified ablation and caused meltwater loss. According to instrumental temperature data from such a high-elevation site, the number of days per year with daily mean air temperature of >0°C is approximately 20, most of which occur during July and August, which means that almost all the annual ablation occurs in July and August. Thus, only data for July and August in each year during 1997–2005 were considered in the evaluation of meltwater loss.

Ablation strength: Values of DDF at the drilling site were calculated at monthly intervals from May–September during 2011–2012. The values fluctuated greatly but were relatively stable in July and August with ranges of 4.73–5.5 and 2.5–3.6 mm °C^{-1} d^{-1}, respectively (Fig. 5). Thus, the amount of melting during 2011–2012 was estimated using the mean DDF values of 5.12 mm °C^{-1} d^{-1} in July and 3.05 mm °C^{-1} d^{-1} in August.

Meltwater refreezing ratio: In China, the MRR of glaciers is usually taken as 10%, which is a value based on limited observations conducted in both the Tien Shan Mountains and the Qilian Mountains (Xie and Liu, 2010). However, the MRR of different glaciers and in different seasons is expected to vary widely. Thus, trials were undertaken in this study to determine an accurate MRR for the drilling site. We tuned the MRR from 0 to 100% at intervals of 1% until the revised ice accumulation with the tuned MRR best matched the instrumental precipitation on the annual scale. Precipitation observations from 11 meteorological stations surrounding the study site (Table 1) were collected to determine the best correlation with the revised ice accumulation. As shown in Figure 6a, the precipitation observed at Tuole displayed the best correlation with the revised ice accumulation, and further detailed analyses (as illustrated in Fig. 6b) indicated that an MRR value of 26% was optimal for the studied site.

Because temperature rise displayed no obvious shift during 1961–1996, ablation intensity and information preservation in the layers of the snow pits did not alter markedly. It can be concluded that meltwater was completely preserved in the snow pit because the total ablation amount was less than the maximum water storage of the snow pit during this period. The annual meltwater loss during 1997–2005 showed a substantial difference of 34.2 mm w.e., that is, ranging from 57.4 mm w.e. (in 2000) to 23.2 mm w.e. (in 2003); the median and mean values were
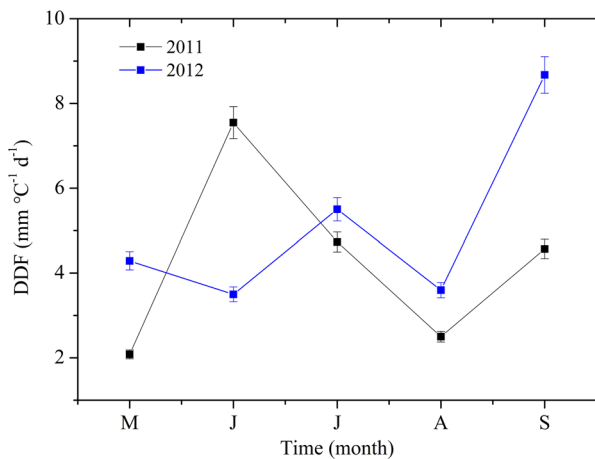

Figure 4. (a) Variation in positive degree days (PDD) and (b) the results of the Mann–Kendall test. The statistic is result of Mann–Kendall test, which includes *UF* and *UB*. *UF* is the forward sequence that follows the normal distribution, indicating the change trend, while *UB* can be denoted by reversing the data series based on the same equation.

Figure 5. Variation in monthly degree day factor (DDF) during 2011–2012 at the drilling site.

54.51 and 43.11 ± 3.75 mm w.e., respectively. The meltwater loss increased during 1999–2000, then decreased until 2003 and then increased again in the following two years (Fig. 7c).

3.3. Precipitation signals from revised annual ice accumulation

Adding S/E and meltwater loss together, the mass loss of the LHG ice core in the northeastern TP was quantified as the revised annual ice accumulation (Fig. 7d). It increased significantly until the 1980s (slope = 16.7, $p < 0.05$), following which it began to decrease. The relative difference was 558.75 mm w.e. between the largest annual ice accumulation in 1992 (768.59 mm w.e.) and the smallest in 1961 (209.83 mm w.e.). The median and mean values were 631.93 and 490.73 ± 125.57 mm w.e., respectively, that is, greater than their original values. The revised range and variance were both broadly unchanged, as were the trend, periodicity and time of the abrupt change. This indicated that the variation of alpine precipitation was well recorded in the mass loss of the LHG ice core.

During 1961–1996, the revised annual ice accumulation was well correlated with the observations recorded at the Tuole and Lenghu meteorological stations ($r = 0.32$, $p < 0.05$), where ice mass loss occurs only via S/E. Correlation with precipitation at Tuole station was stronger ($r = 0.475$), but it failed to pass the confidence test when meltwater loss was taken into account during 1997–2005. Over the entire period, the most significant relationship between the revised annual accumulation and ambient precipitation was detected for Tuole station (Figs 7d and e). The elevation effect on increasing precipitation was notable as a trait of alpine precipitation. It should be noted that qualification of

Table 1. Location and elevation of 11 meteorological stations near the study site

Site name	Longitude (°E)	Latitude (°N)	Elevation (m a.s.l.)
Mazongshan (MZS)	97.02	41.48	1770.4
Dunhuang (DH)	94.68	40.2	1138.7
Anxi (AX)	95.92	40.5	1170.8
Yumenzhen (YMZ)	97.04	40.3	1526
Subei (SB)	94.52	39.31	2137.2
Jiuquan (JQ)	98.29	39.46	1477.2
Tuole (TL)	98.42	38.8	3367
Dachaidan (DCD)	95.37	37.85	3174
Delingha (DLH)	97.37	37.37	2982
Lenghu (LH)	93.2	38.45	2770
Hongliuhe (HLH)	94.4	41.32	1573.8

mass loss promotes understanding of alpine precipitation, especially in high-elevation regions.

4. Discussion

During 1961–2005, the average annual mass loss in the ice core was 95.33 ± 20.56 mm w.e. (minimum: 78.97 mm w.e. in 1967, maximum: 146.67 mm w.e. in 2001), while the average ratio of the revised annual ice accumulation was 21.2 ± 7.7% (minimum: 11.0% in 1992, maximum 44.8% in 2000). Thus, over the entire study period, the average annual S/E was 86.71 ± 3.52 mm w.e. (minimum: 78.97 mm w.e. in 1992, maximum: 95.08 mm w.e. in 1961), while the average ratio of the revised annual ice accumulation was 19.32 ± 6.17% (minimum: 11% in 1974, maximum: 44.79% in 2000). Meanwhile, since 1997, the average annual meltwater loss was 43.11 ± 3.75 mm w.e. (minimum: 23.2 mm w.e. in 2003, maximum: 57.4 mm w.e. in 2000), while the average ratio of the revised annual ice accumulation was 9.21 ± 3.9% (minimum: 4.25% in 2003, maximum: 17.61% in 2000).

4.1. Comparison of S/E on different glaciers

The mass loss of the LHG ice core in the northeastern TP was less than that of a valley glacier (33%) in South America and the Cerro Tapado ice core (50.86%) obtained in the Chilean Andes (Ginot and others, 2006). Most importantly, ice cores drilled on Mt. Naimona'nyi (6050 m a.s.l.) in 2006, Mt. Nyainqentanglha (5850 m a.s.l.) in 2002, and Mt. Geladaindong (5750 m a.s.l.) in 2005 revealed the absence of certain critical reference chemical
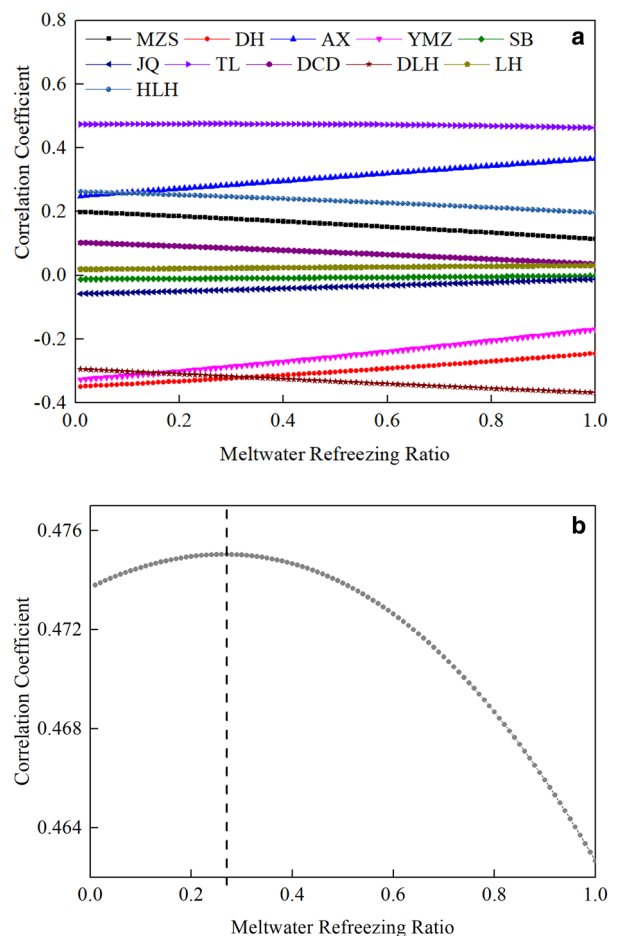

Figure 6. Different scenarios of meltwater refreezing ratio (MRR) at 1% intervals (a) according to the relation between adjacent stations (see Table 1) and (b) the optimal value.
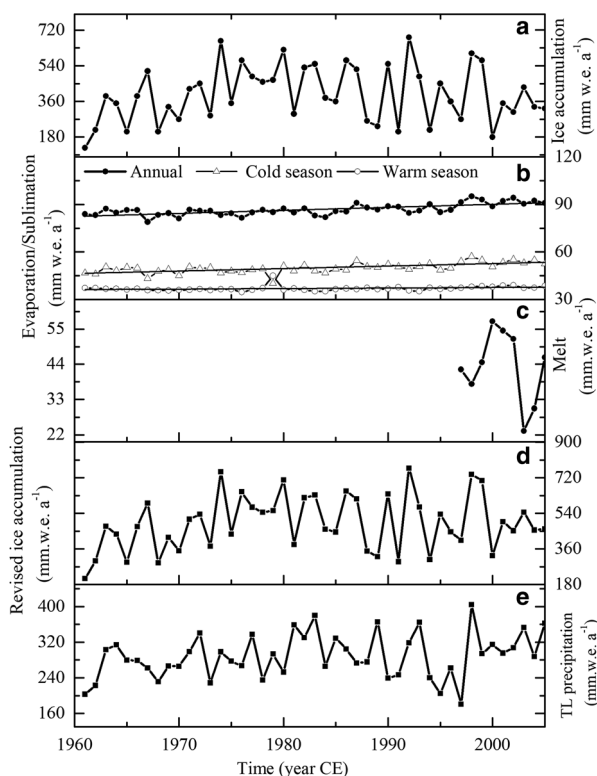
Figure 7. Variations in (a) ice accumulation, (b) S/E loss, (c) meltwater loss, (d) revised ice accumulation and (e) precipitation at Tuole (TL) station during 1961–2005.

peaks (e.g. Tritium), suggesting that mass loss causes shrinkage of the top accumulation zone of glaciers in central and southern parts of the TP (Kang and others, 2015; Zhang and others, 2015).

Owing to the ever-present and increasingly severe mass loss of glaciers, it is necessary to investigate the spatial pattern of S/E and its potential drivers. However, comparison of S/E determined for different locations can be somewhat problematic because of different experimental methodologies, observation times and site elevations. The S/E of many glaciers in different parts of the TP are listed in Table 2. It can be seen that S/E at the drilling site on LHG Glacier No. 12 (86.7 mm w.e.) is similar to that obtained for the Qiyi Glacier and Urumiqi Glacier No. 1; however, it is smaller than that of most glaciers in western, northern, southern and central parts of the TP. There are two exceptions to this pattern: Parlung Glacier No. 94 in the southern TP and Xiao Dongkemadi Glacier in the central TP, where S/E is smaller than that determined for LHG Glacier No. 12. The pattern of S/E of the listed glaciers might reflect the effects of dramatic solar dimming over the southern TP and wind stilling in the northern TP (Zhang and others, 2009; Yang and others, 2014).

In contrast, the Antarctic continent with its cold, dry climate and relatively high temperatures in summer effectively promotes water vapor diffusion from the snow/ice surface to the air such that the latent heat of sublimation/evaporation is the leading energy expenditure (Bintanja and van den Broeke, 1995). The combined processes of surface and blowing snow sublimation are estimated to remove 29 mm w.e. a^{-1} over Antarctica, disposing of approximately 17–20% of the annual precipitation (Déry and Yau, 2002). In the Arctic, especially the Greenland Ice Sheet, total sublimation ranges from $-0.62 \pm 0.25 \times 10^{14}$ to $-1.2 \pm 0.65 \times 10^{14}$ kg a^{-1}, indicating 12 or 23% precipitation loss, respectively (Box and Steffen, 2001). Mass loss from sublimation (32 mm w.e. a^{-1}) at the Greenland Summit (center of dry snow zone: 72°35′N, 38°28′W; 3203 m a.s.l.) is thought to remove approximately 10% of the mass gain from annual precipitation (Cullen and others, 2014). It is important that mass loss by sublimation is not neglected, irrespective of elevation or latitude of the glacier (Potocki and others, 2022).

4.2. Causes of S/E at different regional scales

Pan evaporation at most locations in the Northern Hemisphere has been decreasing over the past several decades (Peterson and others, 1995), and a similar trend has been observed throughout most of China except in the northeast (Liu and others, 2004). The observed decrease in evaporation, which contradicts theoretical analysis that suggests it should increase with the effects of global warming, is known as the pan evaporation paradox (Roderick and Farquhar, 2002). However, the observed decreases are consistent with widespread decreases in solar irradiance, wind speed and diurnal temperature range. In China, the greatest decline has occurred in the northwest, while the lowest decline has been in the southwest, with descending rates of decline moving from the northwest to the south and to the east. This spatial pattern of pan evaporation is anticorrelated with the distribution of summer precipitation, implying that atmospheric humidity plays a critical role in pan evaporation. Air temperature is another important climatic driver because prediction performance can be improved substantially in northwestern China and on the TP through consideration of air temperature in multiple regression models between meteorological parameters and evaporation; however, improvement at the national level has not been realized (Liu and others, 2004). It has been observed that pan evaporation has increased greatly at the stations of Dunhuang and Mazongshan in Gansu Province, which are two nearby stations in the same administrative region as the study site. This is attributed to air temperature increase rather than to wind, that is, thermal factors dominate evaporation (Wang and others, 2010). Some studies have concluded that the diurnal temperature range has stronger correlation than other individual meteorological factors

Table 2. Comparison of sublimation/evaporation (S/E) on different glaciers

Glacier	Location	Accumulation/ablation area	Period	Mannitude (mm w.e.)	Reference
Laohugou Glacier No. 12	Qilian Mountains, Northern TP	Accumulation area	1960–2005	86.7	This study
Shiyi Glacier		Whole glacier	2011.12	100	Fang and others (2015)
Bayi Glacier		Accumulation area	2016–2017	115.1	Guo and others (2018)
Qiyi Glacier		Ablation area	2010.7–2010.10	36	Jiang and others (2010)
Urumqi Glacier No. 1	Tien Shan	Accumulation area	1987–1988	81	Ohno and others (1992)
Qiangtang Glacier No. 1	Central TP	Accumulation area	2013–2016	175.5	Li and others (2018)
Zhadang Glacier	Central TP	Ablation area	2010.12	105	Zhang and others (2016)
Xiao Dongkemadi Glacier	Central TP	Whole glacier	1992	70	Fujita and Ageta (2000)
Palongzangbu Glacier No. 4	Southern TP	Ablation area	2010.12	123	Zhu and others (2015)
Parlung Glacier No. 94	Southern TP	Accumulation area	2005.10	60	Yang and others (2013)
Muztage Ata Glacier No. 15	Western TP	Whole glacier	1980–2012	317	Zhu and others (2018)
Guliya ice cap	Western TP	Whole glacier	2015–2016	123	Li and others (2019)

with pan evaporation in China because the diurnal temperature range is a remarkable reflection of multiple other factors (Liu and others, 2010).

The variation of S/E or that of the latent heat of snow/ice depends on the amount of turbulence at the surface, which is associated with the energy budget (i.e. sunshine duration and air temperature), water vapor transport (i.e. saturation deficit of water vapor and wind speed) and its mediums. Thus, in comparison with other meteorological variables, the gradient of specific humidity, temperature between the air and the snow/ice and wind speed are the most important factors of the climatic forcing behind S/E changes (Sun and others, 2014; Guo and others, 2018). As described earlier, S/E decreases with increasing air temperature during the melting seasons owing to the constraints imposed on its surface temperature by melting, while S/E is much higher during the cold seasons. Thus, annual S/E has increased since the 1960s because the temperature gradient has increased dramatically.

5. Conclusions

This study analyzed a new ice core spanning 1960–2006, obtained from LHG Glacier No. 12 in the western Qilian Mountains of the northeastern TP, using integrated glacier and meteorological observations to assess its climatic reliability and validity. The contributions of primary mass loss from S/E and meltwater loss were quantified using the BAM and the DDM, while minor contributions from both snowdrifting and avalanches were neglected. Analysis revealed that historical variations of precipitation were well recorded in the LHG ice core. During 1961–2005, the average annual mass loss in the ice core was 95.33 ± 20.56 mm w.e. (minimum: 78.97 mm w.e. in 1967, maximum: 146.67 mm w.e. in 2001), while the average ratio of the revised annual ice accumulation was 21.2 ± 7.7% (minimum: 11.0% in 1992, maximum 44.8% in 2000). Thus, over the entire study period, the average annual S/E was 86.71 ± 3.52 mm w.e. (minimum: 78.97 mm w.e. in 1992, maximum: 95.08 mm w.e. in 1961), while the average ratio of the revised annual ice accumulation was 19.32 ± 6.17% (minimum: 11% in 1974, maximum: 44.79% in 2000). Meanwhile, since 1997, the average meltwater loss was 43.11 ± 3.75 mm w.e. (minimum: 23.2 mm w.e. in 2003, maximum: 57.4 mm w.e. in 2000), while the average ratio of the revised annual ice accumulation was 9.21 ± 3.9% (minimum: 4.25% in 2003, maximum: 17.61% in 2000). Using the calculated mass loss, the revised mean, maximum and minimum values of annual accumulation were increased by 95.33, 84.6 and 83.8 mm w.e., respectively, in comparison with the original ice accumulation data. However, both the range and the variance of annual mass loss were effectively unchanged. Additionally, a quantitative formula expressing the relationship between S/E and air temperature at the annual scale was established, providing an improved method for assessment of S/E in the northeastern TP using time series temperature data. The annual variation in revised ice accumulation correlated best with precipitation recorded at Tuole station. The elevation effect on precipitation was remarkable, highlighting the trait of alpine precipitation throughout the entire period. This explorative research developed a method for quantitative assessment of the time-varying mass loss of ice cores, and advanced the reconstruction of long-term precipitation at high elevations. However, certain limitations of this study could be addressed in future work. Most importantly, the dataset of in situ observations should be extended temporally and spatially. Additionally, reanalysis data and satellite data might represent better choices for long-term and spatial reconstruction through data assimilation or bias correction based on in situ measurements (Guo and others, 2022; Srivastava and Azam, 2022). Multisource meteorological data could provide opportunities for improving regional or long-term S/E simulations using physical methods such as the BAM and the Energy Balance Model, while sufficient in situ measurements would benefit calibration and support simplification of model parameters.

References

Andreas EL (1987) A theory for the scalar roughness and the scalar transfer coefficients over snow and sea ice. *Boundary-Layer Meteorology* **38**(1), 159–184. doi: 10.1007/BF00121562

Bintanja R and van den Broeke MR (1995) The surface energy balance of Antarctic snow and blue ice. *Journal of Applied Meteorology and Climatology* **34**(4), 902–926. doi: 10.1175/1520-0450(1995)034%3C0902:TSEBOA%3E2.0.CO;2

Box JE and Steffen K (2001) Sublimation on the Greenland ice sheet from automated weather station observations. *Journal of Geophysical Research: Atmospheres* **106**(D24), 33965–33981. doi: 10.1029/2001JD900219

Braithwaite RJ and Zhang Y (2000) Sensitivity of mass balance of five Swiss glaciers to temperature changes assessed by tuning a degree-day model. *Journal of Glaciology* **46**(152), 7–14. doi: 10.3189/172756500781833511

Cauvy-Frauníe S and 5 others (2016) Ecological responses to experimental glacier-runoff reduction in alpine rivers. *Nature communications* **7**, 12025. doi: 10.1038/ncomms12025

Chen J (2014) *The Research of Summertime Energy and Mass Balance of Laohugou No.12 Glacier*. Lanzhou: Master Thesis, Lanzhou University, pp. 1–70 (in Chinese).

Chen J and 5 others (2018) Effects of clouds on surface melting of Laohugou Glacier No. 12, Western Qilian Mountains, China. *Journal of Glaciology* **64**(243), 89–99. doi: 10.1017/jog.2017.82

Cui X and 6 others (2014) Chemical characteristics and environmental records of a snow-pit at the Glacier No. 12 in the Laohugou Valley, Qilian Mountains. *Journal of Earth Science* **25**(2), 379–385. doi: 10.1007/s12583-014-0426-6

Cui X, Ren J and Qin X (2010) Source of major ions from an ice core of the No. 12 Glacier in Laohugou Valley, Qilian Mountain. *Science in Cold and Arid Regions* **2**(6), 522–528. doi: 10.3724/SP.J.1226.2010.00522

Cullen NJ, Mölg T, Conway J and Steffen K (2014) Assessing the role of sublimation in the dry snow zone of the Greenland ice sheet in a warming world. *Journal of Geophysical Research: Atmospheres* **119**(11), 6563–6577. doi: 10.1002/2014JD021557

Déry SJ and Yau MK (2002) Large-scale mass balance effects of blowing snow and surface sublimation. *Journal of Geophysical Research: Atmospheres* **107**(D23), ACL-8. doi: 10.1002/2014JD021557

Du W, Qin X, Sun W, Liu Y and Hou S (2011) Reconstruction of air temperature at glacier area in mountain – a case of Laohugou glacier area. *Journal of Arid Land Resources and Environment* **25**(10), 149–154 (in Chinese). doi: 10.13448/j.cnki.jalre.2011.10.027

Du W, Qin X, Sun W, Liu Y and Hou S (2012) Wind characteristics in accumulation area of the Laohugou Glacier No.12, Qilian Mountain. *Journal of Glaciology and Geocryology* **34**(1), 29–36 (in Chinese). doi: 1000-0240 (2008)03-0373-07

Du W, Qin X, Kang S, Cui X and Sun W (2016a) Variations in annual accumulation recorded in a Laohugou ice core from the northeastern Tibetan Plateau and their relationship with atmospheric circulation. *Environmental Earth Sciences* **75**(9), 845. doi: 10.1007/s12665-016-5601-x

Du W, Kang S, Qin X, Cui X and Sun W (2016b) Atmospheric insight to climatic signals of δ18O in a Laohugou ice core in the northeastern Tibetan Plateau during 1960–2006. *Sciences in Cold and Arid Regions* **8**(5), 367–377. doi: 10.3724/SP.J.1226.2016.00367

Fang X, Li Z, Bernd W, Gao S and Chen R (2015) Physical energy-balance and statistical glacier melting models comparison and testing for Shiyi Glacier, Heihe River Basin, Qilian Mountains, China. *Journal of Glaciology and Geocryology* **37**(2), 336–350 (in Chinese). doi: 10.7522/j.issn.100-0240.2015.0037

Fisher DA and Koerner RM (1994) Signal and noise in four ice-core records from the Agassiz Ice Cap, Ellesmere Island, Canada: details of the last millennium for stable isotopes, melt and solid conductivity. *The Holocene* **4**(2), 113–120. doi: 10.1177/095968369400400201

Fujita K and Ageta Y (2000) Effect of summer accumulation on glacier mass balance on the Tibetan Plateau revealed by mass-balance model. *Journal of Glaciology* **46**(153), 244–252. doi: 10.3189/172756500781832945

Gabbi J, Carenzo M, Pellicciotti F, Bauder A and Funk M (2014) A comparison of empirical and physically based glacier surface melt models for long-term simulations of glacier response. *Journal of Glaciology* **60**(224), 1140–1154. doi: 10.3189/2014JoG14J011

Gascoin S, Lhermitte S, Kinnard C, Bortels K and Liston GE (2013) Wind effects on snow cover in Pascua-Lama, Dry Andes of Chile. *Advances in Water Resources* **55**, 25–39. doi: 10.1016/j.advwatres.2012.11.013

Ginot P, Kull C, Schotterer U, Schwikowski M and Gäggeler HW (2006) Glacier mass balance reconstruction by sublimation induced enrichment of chemical species on Cerro Tapado (Chilean Andes). *Climate of the Past* **2**(1), 21–30. doi: 10.5194/cp-2-21-2006

Guo W and 6 others (2015) The second Chinese glacier inventory: data, methods and results. *Journal of Glaciology* **61**(226), 357–372. doi: 10.3189/2015JoG14J209

Guo S and 6 others (2018) Simple parameterization of aerodynamic roughness lengths and the turbulent heat fluxes at the top of midlatitude August-One Glacier, Qilian Mountains, China. *Journal of Geophysical Research: Atmospheres* **123**(21), 12–066. https://cp.copernicus.org/articles/2/21/2006/10.1029/2018JD028875.

Guo S, Chen R and Li H (2022) Surface sublimation/evaporation and condensation/deposition and their links to westerlies during 2020 on the August-One Glacier, the Semi-Arid Qilian Mountains of Northeast Tibetan Plateau. *Journal of Geophysical Research: Atmospheres* **127**(11), e2022JD036494. doi: 10.1029/2022JD036494

Hamed KH and Rao AR (1998) A modified Mann–Kendall trend test for autocorrelated data. *Journal of Hydrology* **204**(1–4), 182–196. doi: 10.1016/S0022-1694(97)00125-X

Hou S, Qin D, Yao T, Zhang D and Chen T (2002) Recent change of the ice core accumulation rates on the Qinghai-Tibetan Plateau. *Chinese Science Bulletin* **47**(20), 1746–1749. doi: 10.1007/BF03183321

Huang M and Xie Z (1988) *Snow-Ice Transformation in China: An Introduction to the Glaciers in China*. Beijing: Science Press, pp. 55–68. (in Chinese) ISBN: 7030006526.

Immerzeel WW and Bierkens MFP (2012) Asia's water balance. *Nature Geoscience* **5**(12), 841. doi: 10.1038/ngeo1643

Jiang X, Wang NL, Yang SP, He JQ and Song GJ (2010) The surface energy balance on the Qiyi Glacier in Qilian Mountains during the ablation period. *Journal of Glaciology and Geocryology* **32**(4), 686–695 (in Chinese). doi: 10.3724/SP.J.1037.2010.00186

Johnsen SJ and 5 others (2000) Diffusion of stable isotopes in polar firn and ice: the isotope effect in firn diffusion. *Physics of Ice Core Records* **159**, 121–140.

Kang S and 5 others (2010) Review of climate and cryospheric change in the Tibetan Plateau. *Environmental Research Letters* **5**(1), 015101. doi: 10.1088/1748-9326/5/1/015101

Kang S (2011) Atmospheric circulation and glaciochemical records. *Encyclopedia of Snow, Ice and Glaciers*, Berlin: Springer, pp. 75–76. ISBN: 978-90-481-2641-5.

Kang S and 6 others (2015) Dramatic loss of glacier accumulation area on the Tibetan Plateau revealed by ice core tritium and mercury records. *The Cryosphere* **9**(3), 1213–1222. doi: 10.5194/tc-9-1213-2015

Lanzhou Institute of Glaciology and Geocryology (1988) *Chinese Academy of Sciences: An Introduction to Glaciers in China*. Beijing: Science Press, pp. 1–242 (in Chinese).

Lenaerts JTM, van den Broeke MR, van de Berg WJ, van Meijgaard E and Kuipers Munneke P (2012) A new, high-resolution surface mass balance map of Antarctica (1979–2010) based on regional atmospheric climate modeling. *Geophysical Research Letters* **39**(4), L04501. doi: 10.1029/2011GL050713

Li S, Yao T, Yang W, Yu W and Zhu M (2018) Glacier energy and mass balance in the Inland Tibetan Plateau: seasonal and interannual variability in relation to atmospheric changes. *Journal of Geophysical Research: Atmospheres* **123**(12), 6390–6409. doi: 10.1029/2017JD028120

Li S, Yao T, Yu W, Yang W and Zhu M (2019) Energy and mass balance characteristics of the Guliya ice cap in the West Kunlun Mountains, Tibetan Plateau. *Cold Regions Science and Technology* **159**, 71–85. doi: 10.1016/j.coldregions.2018.12.001

Liu B, Xu M, Henderson M and Gong W (2004) A spatial analysis of pan evaporation trends in China, 1955–2000. *Journal of Geophysical Research: Atmospheres* **109**(D15102). doi: 10.1029/2004JD004511

Liu M, Shen Y, Zeng Y and Liu C (2010) Trend in pan evaporation and its attribution over the past 50 years in China. *Journal of Geographical Sciences* **20**(4), 557–568. doi: 10.1007/s11442-010-0557-3

Mölg T, Großhauser M, Hemp A, Hofer M and Marzeion B (2012) Limited forcing of glacier loss through land-cover change on Kilimanjaro. *Nature Climate Change* **2**(4), 254. doi: 10.1038/nclimate1390

Mott R, Vionnet V and Grünewald T (2018) The seasonal snow cover dynamics: review on wind-driven coupling processes. *Frontiers in Earth Science* **6**, 197. doi: 10.3389/feart.2018.00197

Noël B and 6 others (2016) A daily, 1 km resolution data set of downscaled Greenland ice sheet surface mass balance (1958–2015). *The Cryosphere* **10**(5), 2361–2377. doi: 10.5194/tc-10-2361-2016

Ohno H, Ohata T and Higuchi K (1992) The influence of humidity on the ablation of continental-type glaciers. *Annals of Glaciology* **16**, 107–114. doi: 10.3189/1992AoG16-1-107-114

Oke TR (1987) *Boundary layer climates*, 2nd (ed.) New York: Routledge. London and Wiley, pp. 435.

Peterson TC, Golubev VS and Groisman PY (1995) Evaporation losing its strength. *Nature* **377**(6551), 687. doi: 10.1038/377687b0

Potocki M and 10 others (2022) Mt. Everest's highest glacier is a sentinel for accelerating ice loss. *NPJ Climate and Atmospheric Science* **5**(1), 1–8. doi: 10.1038/s41612-022-00230-0

Pramanik A, Kohler J, Schuler TV, van Pelt W and Cohen L (2019) Comparison of snow accumulation events on two High Arctic glaciers to model-derived and observed precipitation. *Polar Research* **38**(3364). doi: 10.33265/polar.v38.3364

Qin D and 6 others (2017) Cryospheric science: research framework and disciplinary system. *National Science Review* **5**(2), 255–268. doi: 10.1093/nsr/nwx108

Reijmer CH, van den Broeke MR, Fettweis X, Ettema J and Stap LB (2012) Refreezing on the Greenland ice sheet: a comparison of parameterizations. *The Cryosphere* **6**, 743–762. doi: 10.5194/tc-6-743-2012

Roderick ML and Farquhar GD (2002) The cause of decreased pan evaporation over the past 50 years. *Science* **298**(5597), 1410–1411. doi: 10.1126/science.1075390-a

Schulz O and de Jong C (2004) Snowmelt and sublimation: field experiments and modelling in the High Atlas Mountains of Morocco. *Hydrology and Earth System Sciences Discussions* **8**(6), 1076–1089. doi: 10.5194/hess-8-1076-2004

Srivastava S and Azam M (2022) Mass-and energy-balance modeling and sublimation losses on Dokriani Bamak and Chhota Shigri glaciers in Himalaya since 1979. *Frontiers in Water* **4**, 47. doi: 10.3389/frwa.2022.874240

Stichler W and 6 others (2001) Influence of sublimation on stable isotope records recovered from high-altitude glaciers in the tropical Andes. *Journal of Geophysical Research: Atmospheres* **106**(D19), 22613–22620. doi: 10.1029/2001JD900179

Su H, Wei W and Han P (2003) Changes in air temperature and evaporation in Xinjiang during the recent 50 years. *Journal of Glaciology Geocryology* **25**(2), 174–178 (in Chinese). doi: 1000-0240(2003)02-0174-05

Sun W and 6 others (2012) The surface energy budget in the accumulation zone of the Laohugou Glacier No. 12 in the western Qilian Mountains, China, in summer 2009. *Arctic, Antarctic, and Alpine Research* **44**(3), 296–305. doi: 10.1657/1938-4246-44.3.296

Sun W and 6 others (2014) Ablation modeling and surface energy budget in the ablation zone of Laohugou Glacier No. 12, western Qilian Mountains, China. *Annals of Glaciology* **55**(66), 111–120. doi: 10.3189/2014AoG66A902

Sun W and 6 others (2017) The response of surface mass and energy balance of a continental glacier to climate variability, western Qilian Mountains, China. *Climate Dynamics* **50**(9–10), 3557–3570. doi: 10.1007/s00382-017-3823-6

Sun, Q and 5 others (2018) A review of global precipitation data sets: data sources, estimation, and intercomparisons. *Reviews of Geophysics* **56**(1), 79–107. doi: 10.1002/2017RG000574

Taylor S and 5 others (2001) Isotopic evolution of a seasonal snowpack and its melt. *Water Resources Research* **37**(3), 759–769. doi: 10.1029/2000WR900341

van den Broeke M and 6 others (2009) Partitioning recent Greenland mass loss. *Science* **326**(5955), 984–986. doi: 10.1029/2000WR900341

van Pelt WJJ, Oerlemans J, Reijmer CH, Pohjola VA, Pettersson R and van Angelen JH (2012) Simulating melt, runoff and refreezing on Nordenskiöldbreen, Svalbard, using a coupled snow and energy balance model. *The Cryosphere* **6**(3), 641–659. doi: 10.5194/tc-6-641-2012

Wang SP, Zhang CJ and Han YX (2010) Trend of potentia1evapotranspiration and pan evaporation and their main impact factors in different climate regions of Gansu province. *Journal of Desert Research* **30**(3), 675–680 (in Chinese). doi: 10.3788/HPLPB20102207.1462

Xie Z and Liu C (2010) *Glaciology Introduction*. Shanghai: Shanghai Popular Science Press, pp. 1–490 (in Chinese).

Yang W and 5 others (2013) Mass balance of a maritime glacier on the southeast Tibetan Plateau and its climatic sensitivity. *Journal of Geophysical Research: Atmospheres* **118**(17), 9579–9594. doi: 10.1002/jgrd.50760

Yang K and 5 others (2014) Recent climate changes over the Tibetan Plateau and their impacts on energy and water cycle: a review. *Global and Planetary Change* **112**, 79–91. doi: 10.1016/j.gloplacha.2013.12.001

Yao T and 5 others (1996) Climatological significance of δ^{18}O in north Tibetan ice cores. *Journal of Geophysical Research: Atmospheres* **101** (D23), 29531–29537. doi: 10.1029/96JD02683

Yao T and 6 others (2012) Different glacier status with atmospheric circulations in Tibetan Plateau and surroundings. *Nature Climate Change* **2**(9), 663. doi: 10.1038/nclimate1580

You Q and 6 others (2010) Relationship between temperature trend magnitude, elevation and mean temperature in the Tibetan Plateau from homogenized surface stations and reanalysis data. *Global and Planetary Change* **71**(1–2), 124–133. doi: 10.1016/j.gloplacha.2010.01.020

You Q and 6 others (2014) Comparison of NCEP/NCAR and ERA-40 total cloud cover with surface observations over the Tibetan Plateau. *International Journal of Climatology* **34**(8), 2529–2537. doi: 10.1002/joc.3852

You Q, Min J, Zhang W, Pepin N and Kang S (2015) Comparison of multiple datasets with gridded precipitation observations over the Tibetan Plateau. *Climate Dynamics* **45**(3–4), 791–806. doi: 10.1007/s00382-014-2310-6

You Q, Bao Y, Jiang Z, Pepin N and Moore GWK (2019) Surface pressure and elevation correction from observation and multiple reanalyzes over the Tibetan Plateau. *Climate Dynamics* **53**(9–10), 5893–5908. doi: 10.1007/s00382-019-04905-y

Yu G and 6 others (2014) Post-depositional process features of the insoluble microparticles on the Laohugou Glacier No.12, Qilian Mountains. *Journal of Glaciology and Geocryology* **36**(6), 1394–1402 (in Chinese). doi: 10.7522/j.issn.1000-0240.2014.0166

Zhang X, Ren Y, Yin ZY, Lin Z and Zheng D (2009) Spatial and temporal variation patterns of reference evapotranspiration across the Qinghai-Tibetan Plateau during 1971–2004. *Journal of Geophysical Research: Atmospheres* **114**(D15105). doi: 10.1029/2009JD011753

Zhang Q, Kang S, Gabrielli P, Loewen M and Schwikowski M (2015) Vanishing high mountain glacial archives: challenges and perspectives. *Environmental Science & Technology* **49**(16), 9499–9500. doi: 10.1021/acs.est.5b03066

Zhang G, Kang S, Cuo L and Qu B (2016) Modeling hydrological process in a glacier basin on the central Tibetan Plateau with a distributed hydrology soil vegetation model. *Journal of Geophysical Research: Atmospheres* **121**(16), 9521–9539. doi: 10.1002/2016JD025434

Zhang Y and 6 others (2017) Characteristics of black carbon in snow from Laohugou No. 12 glacier on the northern Tibetan Plateau. *Science of the Total Environment* **607**, 1237–1249. doi: 10.1016/j.scitotenv.2017.07.100

Zhou J and 6 others (2013) Simulating the cold regions hydrological processes in northwest China with modular modeling method. *Journal of Glaciology and Geocryology* **35**(2), 389–400 (in Chinese). doi: 10.7522/j.issn.1000-0240.2013.0047

Zhou S, Nakawo M, Hashimoto S and Sakai A (2008) The effect of refreezing on the isotopic composition of melting snowpack. *Hydrological Processes: An International Journal* **22**(6), 873–882. doi: 10.1002/hyp.6662

Zhu M and 5 others (2015) Energy-and mass-balance comparison between Zhadang and Parlung No. 4 glaciers on the Tibetan Plateau. *Journal of Glaciology* **61**(227), 595–607. doi: 10.3189/2015JoG14J206

Zhu M and 6 others (2018) Reconstruction of the mass balance of Muztag Ata No. 15 glacier, eastern Pamir, and its climatic drivers. *Journal of Glaciology* **64**(244), 259–274. doi: 10.1017/jog.2018.16